Journal of Applied Electrochemistry **31**: 495–500, 2001.

Electrochemical properties of composites based on nanocrystalline anatase (TiO_2) and copper compounds (CuBr, CuO)

Y. MASSIANI, A. GARNIER, M. EYRAUD and P. KNAUTH*
Laboratoire des Matériaux Divisés, Revêtements, Electrocéramiques (MADIREL, UMR 6121 CNRS-Université de Provence), Centre St Charles, 13331 Marseille Cedex 3, France
*(*author for correspondence)*

Received 11 November 2000; accepted in revised form 29 January 2001

Key words: CuBr, CuO, Mott–Schottky analysis, nanocrystalline, TiO_2

Abstract

The electrochemical properties in aqueous solution of composite materials made from nanocrystalline anatase TiO_2 with CuBr and CuO are reported. CuO–TiO_2 composite samples are prepared by a novel route based on oxidation of CuBr–TiO_2. The corrosion of CuBr–TiO_2 composite electrodes prevents a detailed electrochemical analysis. The data on CuO–TiO_2 composites are consistent with the presence of a surface layer of TiO_2 nanoparticles. A Mott–Schottky analysis gives a flat-band potential of −0.5 V/NHE (pH = 6) and a low carrier density of 10^{14} cm^{-3}.

1. Introduction

Interfaces between p- and n-type semiconductors have great technological importance at the heart of microelectronics [1]. Interfaces also play a significant role in other domains of materials research, such as solid state ionics [2]. We have investigated the interfacial properties of ionic and mixed conductors, in the form of polycrystalline [3, 4], thin-film [5, 6], nanocrystalline [7] and composite [8] materials. All these solids have a complex microstructure, so that the priority is given to simple binary compounds with well-defined chemical and physical properties.

Given its chemical stability, absence of toxicity and tuneable semiconductor properties, nanocrystalline TiO_2 has many applications, notably in the photoelectrochemical domain, as electrode material in rechargeable lithium ion batteries [9], in electrochromic devices [10] and in dye-sensitised solar cells [11, 12]. An 'all-solid-state' dye-sensitised solar cell was proposed in 1998 [13], based on a mixture of CuI with dye-sensitised nanocrystalline anatase particles. This new development stimulated interest in obtaining more information on composites of copper(I) halides with nanocrystalline anatase. Several studies were devoted to composites with CuBr matrix, incorporating dispersed nanocrystalline TiO_2 particles with the anatase structure [14, 15]. For several reasons, the mixed conductor CuBr is an ideal matrix material in model composites with TiO_2. (1) CuBr is a relatively soft material that can be compressed at room temperature to high density composites (> 90% of theoretical density). (2) The high Cu^+ ion mobility facilitates the establishment of equilibrium conditions at the interfaces. (3) CuBr is non-hygroscopic and more stable than CuI. (4) Ternary compounds with anatase or solid solutions are not formed under our experimental conditions.

We have previously reported a significant increase in the ionic conductivity of CuBr–TiO_2 composites with moderate volume fraction f of TiO_2 ($0.04 < f < 0.25$) compared to pure CuBr [15]. The conductivity enhancement can be interpreted by the formation of ionic space charge regions near the heterointerfaces, resulting from an 'internal' adsorption phenomenon of Cu^+ ions on the cationophilic anatase surfaces [15]. With addition of sufficient TiO_2 ($f > 0.04$), the space charge regions can percolate through the macroscopic composite, because the anatase nanoparticles tend to form continuous layers around the large CuBr grains. For large TiO_2 content ($f > 0.25$), continuous layers of insulating TiO_2 nanoparticles are formed around the CuBr grains, which interrupt the conduction paths of Cu^+ ions: the ionic conductivity drops sharply after this second percolation threshold. The experimental dependence of conductivity vs second phase content was simulated numerically [16]: the obtained bell-shaped curve was in good agreement with the experimental data. The percolation of TiO_2 particles is also important for the dye-sensitised solar cell based on nanocrystalline anatase, because no significant space charge region exists inside anatase nanoparticles and only majority carriers, i.e. electrons, are transported through the anatase to the current-collecting back-contact [17].

The purpose of the present work was to determine the electrochemical properties of CuBr–TiO_2 composites in aqueous electrolyte. This study follows previous

experiments on polycrystalline CuBr electrodes [18]. Furthermore, we show how the CuBr–TiO_2 samples can be transformed into a CuO–TiO_2 composite by annealing in air at reduced temperature. First results on this oxide–oxide mixture are also reported.

2. Experimental

2.1. *Composite preparation*

The ceramic samples were obtained from pure copper(I) bromide powder (99.999%, Aldrich) and titanium dioxide, prepared by the sulfate process with calcination at 300 °C (Bayer) [19]. The TiO_2 powder was phase-pure nanocrystalline anatase with an average grain size of 20 nm, determined by X-ray diffraction applying Scherrer's equation and by adsorption measurements following the BET technique. A wet chemical analysis of more than 20 elements revealed impurity sodium as principal (1300 ppm), remaining from the precipitation process [15].

Appropriate amounts of the two phases were thoroughly mixed together and pressed into discs under 400 MPa at room temperature. Given the mechanical softness of the ionic conductor CuBr, composite samples with densities above 90% of theoretical, could be obtained by this technique [15]. The residual porosity was sufficiently low so that the ceramics were impermeable to the electrolytic solution.

The discs were annealed at 350 °C for several hours to release stresses and eliminate transient defects due to the compression. If the annealing was done under pure argon, the CuBr–TiO_2 composition was retained. If the sample was annealed under oxidising conditions, for example in air, a complete oxidation of CuBr into CuO was noticed (see below). The different preparation steps were accompanied by a structural analysis using X-ray diffraction (Siemens D5000 diffractometer, CuK_α radiation, $\lambda = 0.15405$ nm) and optical microscopy.

2.2. *Electrochemical characterization*

The electrochemical measurements were performed in a three-electrode cell, with a large gold counter electrode and a saturated sulfate reference electrode (SSE). The electrolyte was a de-aerated aqueous solution of Na_2SO_4 (0.5 M), continously flushed with argon gas. The electrolytic solutions were prepared with high-purity water (ρ=18.2 MΩ cm). The pH of the solution was measured with a pH meter; an average pH value of 6.0 ± 0.1 was maintained throughout the experiments. This is not far from the point of zero charge of TiO_2, inside the large scatter of literature data (e.g. pH=4.7 [20] or 6.7 [21]).

The 0.1–0.2 cm thick composite discs were mounted using epoxy resin with a circular electrode area of 1 cm^2. The back contact was made using a copper wire and silver epoxy paint, following a procedure that gave a good ohmic contact in the case of a pure copper(I) bromide electrode [18]. The copper wire was isolated from the solution with a glass tube embedded in the resin. The electrode surface was carefully polished with diamond paste before the measurements.

The dc current–voltage characteristics and ac impedance spectra were recorded in dim light using an electrochemical interface (Solartron 1287) and a frequency response analyser (Solartron 1260). The linear sweep polarizations and cyclic voltammograms were recorded with a scan rate between 1 and 10 mV s^{-1}. The scans were made from anodic to cathodic potentials. The impedance spectra were measured with a dc bias between +1 and −2 V/SSE in 0.1 V steps. Prior to each measurement, the electrodes were equilibrated for 1 h at the new potential. The amplitude of the ac voltage was 10 mV and the frequency ranged from 10^6 to 10^{-1} Hz.

3. Results and discussion

3.1. *Preparation and structure*

The X-ray diffraction pattern of a CuBr–TiO_2 composite ceramic ($f(TiO_2)$=0.26) after compression and annealing under argon is shown in Figure 1A: all peaks correspond to anatase and γ-CuBr. New lines or line shifts are not observed, indicating the absence of reactions or significant intermixing between CuBr and anatase. According to X-ray line broadening, the grain size of the nanocrystalline anatase remains unchanged during the preparation procedure with an average value of 20 nm. There is no indication for any formation of the rutile phase. These results are expected, since the annealing is done at 350 °C, a temperature insufficient for grain growth or phase transformation in TiO_2 [22].

The complete oxidation of CuBr after annealing in air is demonstrated by X-ray diffraction: the oxidised samples show only peaks of CuO (tenorite phase) and anatase with no evidence of ternary phases or formation of extended solid solutions (Figure 1B). Lines from Cu_2O, rutile TiO_2 or remaining CuBr are absent.

This oxidation technique is a novel way to synthesise oxide composite ceramics without open porosity. The resulting pellets are impermeable to electrolytes. As a result of low processing temperatures, nanocrystalline grain size of TiO_2 is maintained and no formation of copper titanates is observed.

3.2. *Electrochemical properties: CuBr–TiO_2 composites*

In the following, all potentials are indicated vs the normal hydrogen electrode (NHE). The correspondence between the schemes of solid state physics and electrochemistry can be established considering that the potential of the normal hydrogen electrode lies at −4.5 V below the vacuum electron level [23]. Figure 2 shows the typical dc current–voltage behavior of a CuBr–TiO_2 composite electrode ($f(TiO_2)$=0.26, top) in comparison with a polycrystalline CuBr electrode

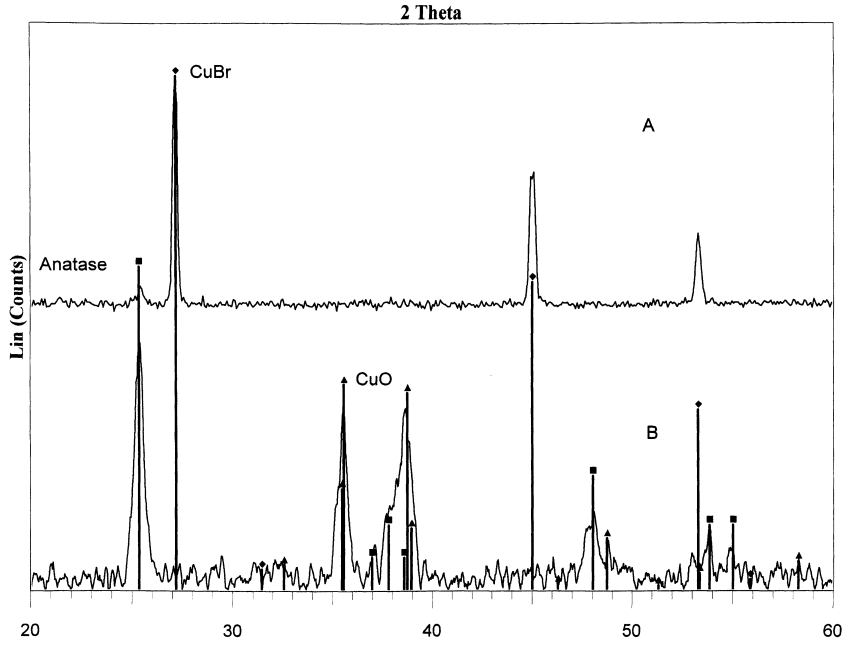

Fig. 1. X-ray diffraction patterns ($\lambda(CuK_\alpha)$=0.15405 nm) of composite samples prepared from CuBr and TiO_2. (A) After annealing at 350 °C under argon, all peaks correspond to CuBr ((◆) JPCDS no 06–0292) or anatase ((■) JPCDS no 21–1272). (B) After annealing in air, the peaks correspond to CuO ((▲) Tenorite phase, JPCDS no 05–0661) or anatase.

(bottom). It is obvious that anodic and cathodic currents for CuBr–TiO_2 are several orders of magnitude larger than those of pure CuBr, due to an enhanced dissolution of the electrode. However, there is also a shift from the p-type behaviour of pure CuBr [18] to an n-type behaviour of the composite (anodic blocking). According to the potential value, the cathodic currents cannot be attributed to proton reduction (E_{eq} = −0.36 V/NHE). They are ascribed to the reduction of Cu^{2+} ions present in the solution due to previous anodic dissolution of the electrode. A large increase in cathodic current is observed when Cu^{2+} ions are voluntarily added to the electrolyte (0.5 M $CuSO_4$), which is consistent with this hypothesis.

The corresponding impedance spectra (Figure 3) confirm this conjecture. The 'bulk' resistance of the composite electrode can be obtained from the high frequency intercept of the observed semi-circle. In the complex impedance plane, a non-ideal semi-circle can be represented by a parallel circuit of a resistance (R) and a constant-phase element (CPE). The impedance of the CPE can be written [24]:

$$Z_{CPE} = Y_0(i\omega)^{-n} \quad (1)$$

Y_0 is a constant prefactor, ω is the angular frequency and i the imaginary unit. The fractional exponent n indicates the physical nature of the element: $n = 0$ corresponds to a pure resistance and $n = 1$ to a pure capacitance. In an elementary model, R represents the charge transfer resistance and can be estimated from the semi-circle diameter. In Table 1, the interfacial resistance data obtained for different CuBr–TiO_2 electrodes in solution are compared to 'all-solid' measurements made on Cu/CuBr–TiO_2/Cu cells. 'All-solid' measurements with copper electrodes gave much larger charge transfer resistances. Furthermore, the charge transfer resistance in solution is orders of magnitude smaller for

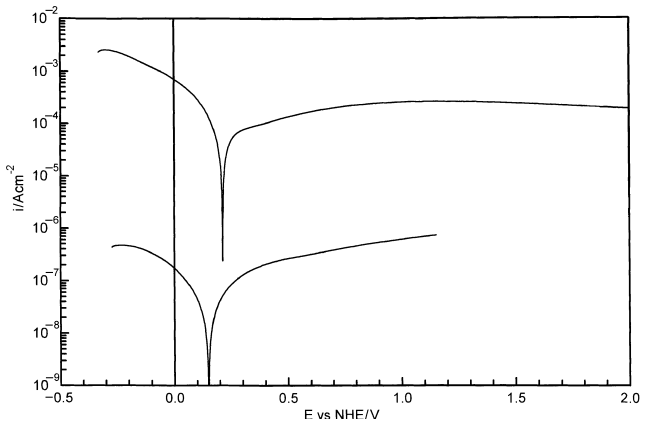

Fig. 2. Dc current–voltage behavior of a CuBr–TiO_2 composite ($f(TiO_2)$=0.26, top) and comparison with polycrystalline CuBr (bottom). Scan rate: 1 mV s^{-1}.

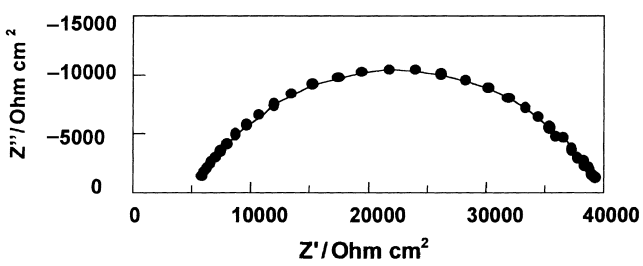

Fig. 3. Impedance spectrum of a CuBr–TiO_2 composite ($f(TiO_2)$= 0.26).

Table 1. Interfacial resistance R_{int} of CuBr–TiO_2 composites with different volume fraction f of TiO_2 determined in solution (liquid junction) or by 'all-solid' measurements (copper electrodes)

$f(TiO_2)$	$R_{int}/k\Omega\ cm^2$	
	Liquid junction	Copper electrodes
0.048		8000
0.098		3600
0.108	5	
0.111		7000
0.131		7500
0.160		500
0.191	47	
0.240	400	
0.264	43	

CuBr–TiO_2 electrodes than for pure CuBr [18]. These discrepancies are indicative of the dissolution of the composite electrode in solution. The corresponding CPE ($n \approx 0.7$) can be attributed to distributed capacitances, with values typical of semiconductors ($\approx 10^{-7}$ F/cm^{-2}).

Several other non-aqueous and aprotic electrolytes were investigated in order to reduce the electrode corrosion, but without success: solutions in acetone and toluene had too large an electrical resistance, CuBr was too soluble in acetonitrile and its derivatives. The experiments were discontinued at this point, because it became apparent that the intended Mott–Schottky analysis was impossible. The rapid electrode corrosion might be related to the rougher surface and slightly larger porosity that increase the active surface area.

3.3. *Electrochemical properties: CuO–TiO_2 composites*

3.3.1. *Dc current–voltage characteristics*

The linear polarization sweep in Figure 4 shows the typical current–voltage behavior of CuO–TiO_2 electrodes. This response is qualitatively similar to that of CuBr–TiO_2 composites, but with much lower currents. The I–V curves show the typical behaviour of a n-type semiconductor. The anodic current above 1.5 V/NHE is characteristic of oxygen evolution from aqueous solution. It is related to hole tunnelling at very large band bending in a n-type semiconductor (inversion layer). The small cathodic current peak in the range −0.2 V/NHE is only observed after anodic oxidation of the electrode. Analogous experiments to those described for CuBr–TiO_2 composites showed that the current is due to the reduction of Cu^{2+} ions present in the solution after prior anodic dissolution of the electrode. This reduction peak becomes larger, if the protective surface layer of TiO_2 is removed by prolonged polishing of the electrode.

The large cathodic current observed below −0.7 V/NHE corresponds to electron accumulation. Several cathodic reactions are conceivable. (1) CuO reduction into Cu_2O is feasible below 0.16 V/NHE [25]. (2) Hydrogen evolution is thermodynamically possible below −0.36 V/NHE at pH=6. (3) Cation insertion into a n-type semiconductor compound is in principle possible below its flat-band potential. Li^+ insertion into anatase has been observed experimentally [26, 27]. Given the larger cation radius, the corresponding Na^+ insertion is improbable in bulk anatase, although it might be possible in subsurface regions (M. Koudriachova, personal communication).

To have a better insight into the reactions, cyclic voltammograms were made. They showed a large convoluted cathodic current below −1 V/NHE and three different processes on the anodic side (Figure 5). The hysteresis in the cathodic part shows that proton reduction can not be the only cathodic process. In this case, the forward and the backward current would be similar. The different amounts of charge for cathodic and anodic processes also indicate side reactions. The first oxidation peak starts at about −0.3 V/NHE, whatever the scan rate. This might correspond to sodium extraction, but more work is necessary to confirm this. The second peak may be attributable to hydrogen oxidation. The peak area observed above 0.5 V/NHE increases with decreasing scan rate. The disappearance of the oxygen evolution at high anodic potentials indicates a change in electrode surface

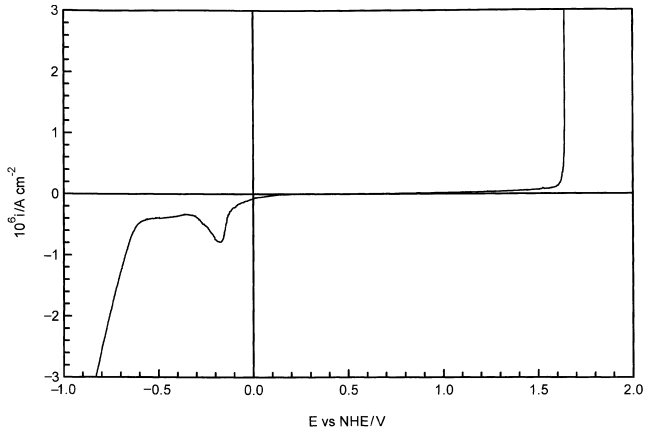

Fig. 4. Dc current–voltage behavior of a CuO–TiO_2 composite ($f(TiO_2)$=0.45). Scan rate: 1 mV s^{-1}.

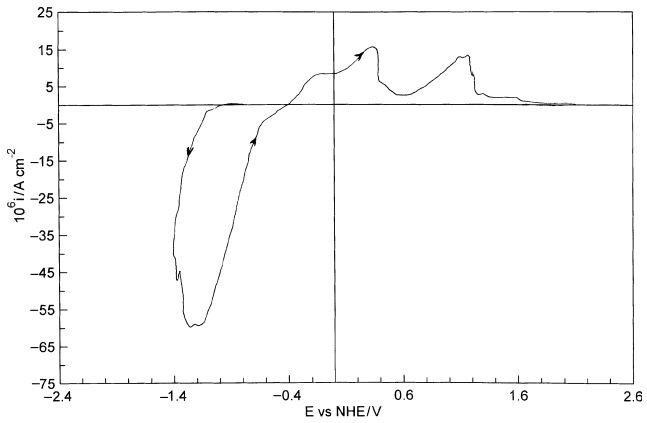

Fig. 5. Cyclic voltammogram of CuO–TiO_2 composite electrodes. Scan rate: 10 mV s^{-1}.

composition. The third peak is most probably related to the oxidation of previously formed Cu_2O. Moreover, the red coloration of the electrode after long-time polarization at cathodic potentials confirms the formation of Cu_2O during reduction with deterioration of the electrode performance. Similar observations have been reported in the literature [28]. Cu_2O was, however, not detected by X-ray diffraction, probably because the oxide is highly defective.

3.3.2. *Impedance spectra and Mott–Schottky analysis*

Typical impedance spectra of a CuO–TiO_2 composite electrode ($f(TiO_2) = 0.45$) are shown in Figures 6 and 7. Figure 6 corresponds to the blocking region ($E = 0.942$ V/NHE) and Figure 7 to the cathodic region ($E = -0.658$ V/NHE), where large currents are observed. The spectra can be interpreted by an equivalent circuit consisting of a series alignment of two parallel elements [resistance (R) + constant-phase element (CPE)].

The high frequency arc does not depend on the bias voltage and is attributable to the 'bulk' of the composite electrode. The 'bulk' CPE is very near an ideal capacitance ($n > 0.9$). Given the small electrical resistivity of CuO ($\rho = 16\ \Omega$ cm [28]), the large 'bulk' resistance of the composite (typically several MΩ, Figures 6–7) can only be understood if insulating TiO_2 forms continuous layers. Previous measurements on nanocrystalline anatase ceramics, made from identical precursor TiO_2 at 500 °C in air gave a resistivity $\rho \approx 10^6\ \Omega$ cm and an activation energy below 1 eV [7]. Using these data, the extrapolated resistivity at 300 K in air is $\rho \approx 10^{13}\ \Omega$ cm. Assuming a thickness of the TiO_2 layer below 20 nm, a resistance below 20 MΩ can be estimated, which is not in contradiction with the experiment. This interpretation is further strengthened by simulations [16], showing that at $f > 0.25$, TiO_2 nanoparticles form continuous layers at the surface of the grains of CuBr. Using our particular oxidation technique at reduced temperature, the initial microstructure of CuBr–TiO_2 composites remains essentially unchanged in CuO–TiO_2 composites.

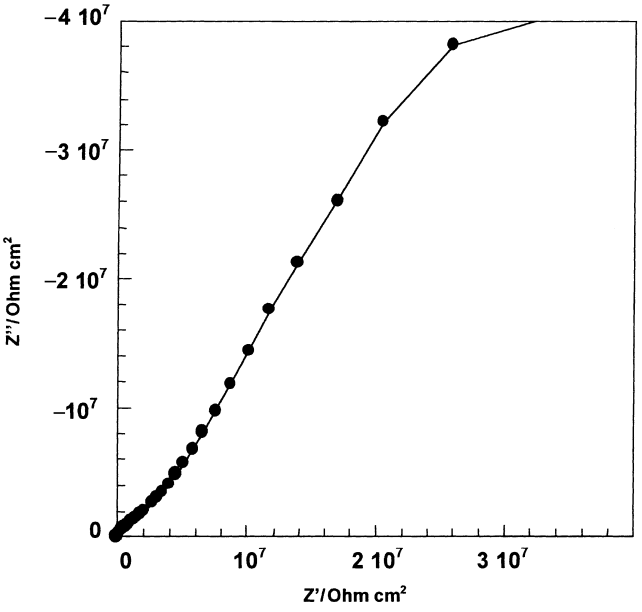

Fig. 6. Impedance spectrum of a CuO–TiO_2 composite ($f(TiO_2) = 0.45$) in the anodic blocking region ($E = 0.942$ V/NHE).

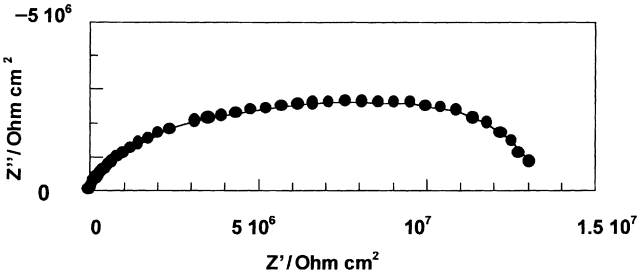

Fig. 7. Impedance spectrum of a CuO–TiO_2 composite ($f(TiO_2) = 0.45$) in the cathodic region ($E = -0.658$ V/NHE).

The low frequency response, corresponding to the composite electrode/electrolytic solution interface, can also be described by a parallel (R–CPE) element. As expected, the respective charge transfer resistances are relatively small in the domain of large cathodic currents (Figure 7). In the potential range corresponding to blocking conditions ($0 < U$ (V/NHE) < 1, Figure 6), the charge transfer resistance is very large. The CPE ($n \approx 0.7$) can again be attributed to distributed capacitances. In the case of charge carrier depletion near the interface with the electrolytic solution, the interfacial capacitances can be used for a Mott–Schottky analysis. According to the Mott–Schottky relation (2), the depletion layer capacitance C of a n-type semiconductor is given by:

$$C^{-2} = 2(E - E_{fb})/(\varepsilon\varepsilon_0\ eN) \qquad (2)$$

Here, E is the electrode potential, E_{fb} the flat-band potential, $\varepsilon\varepsilon_0$ the electrical permittivity, e the elementary charge and N the ionised acceptor/donor concentration (depending on the type of the semiconductor).

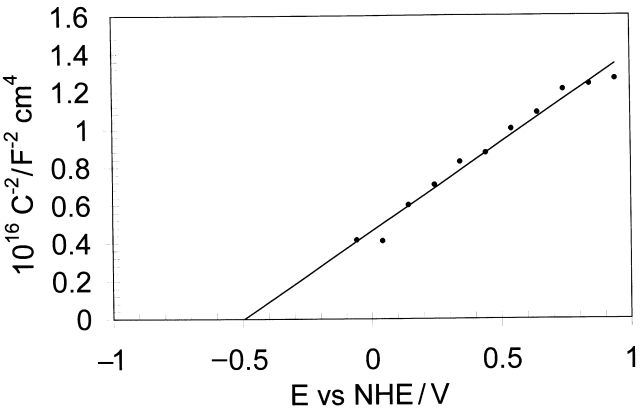

Fig. 8. Mott–Schottky plot for a CuO–TiO_2 composite ($f(TiO_2) = 0.45$)

A plot of the inverse square of the interfacial capacitance data against the electrode potential E (Figure 8) gives a straight line with positive slope, indicative of n-type semiconductor behaviour. The flat-band potential can be extrapolated at the intersection of the straight line with the abscissa: $E_{fb} = -(0.5 \pm 0.1)$ V/NHE. This value is in agreement with the flat-band potential of anatase at pH = 6. The pH dependence of the flat-band potential of anatase can be expressed as (R. Van de Krol, pers. comm.):

$$E_{fb}(\text{V/NHE}) = -0.16 - 0.06\,\text{pH} \quad (3)$$

This equation gives E_{fb}=−0.52 V/NHE at pH = 6.

Using the dielectric constant of anatase ($\varepsilon = 55$ [29]), the ionised donor concentration is: $N_D=(2 \pm 1)10^{14}$ cm^{-3}. This very low carrier density compared with the usual values for anatase is due to charge carrier depletion of the nanocrystallites [30, 31], possibly by contact with p-type CuO. In principle, nanocrystals can be fully depleted of charge carriers, i.e. electrons in n-type TiO_2, when the Debye length λ becomes comparable to the particle size:

$$\lambda = (kT\varepsilon\varepsilon_0/e^2N_D)^{1/2} \quad (4)$$

For a donor density of 10^{14} cm^{-3}, a Debye length of 800 nm can be calculated. Schoonman and coworkers investigated depleted two-layer semiconductor composites of indium-doped tin oxide/anatase with TiO_2 layer thickness up to 120 nm [29]. We believe that our experiments give another example of carrier depletion in nanocrystalline materials.

4. Conclusions

The electrochemical investigation of composite electrodes based on copper compounds and nanocrystalline anatase is complicated by dissolution of the copper compounds. Dc current–voltage characteristics and impedance spectra are consistent with the hypothesis of a continuous surface layer of nanocrystalline anatase particles that protects the electrodes and determines the electrochemical properties in solution. The Mott–Schottky analysis gives low carrier densities in the nanocrystalline anatase particles.

References

1. S.M. Sze, 'Physics of Semiconductor Devices', (Wiley, New York, 1981).
2. J. Maier, *Prog. Solid State Chem.* **23** (1995) 171.
3. S. Villain, M.-A. Desvals, G. Clugnet and P. Knauth, *Solid State Ionics* **83** (1996) 191.
4. P. Knauth, Y. Massiani and M. Pasquinelli, *Phys. Stat. Sol.* **165** (1998) 461.
5. J.-L. Seguin, M. Bendahan, G. Lollmun, M. Pasquinelli and P. Knauth, *Thin Solid Films* **323** (1998) 31.
6. P. Lauque, M. Bendahan, J.-L. Seguin, M. Pasquinelli and P. Knauth, *J. Europ. Ceram. Soc.* **19** (1999) 823.
7. P. Knauth and H.L. Tuller, *J. Appl. Phys.* **85** (1999) 897.
8. M.-A. Desvals and P. Knauth, *J. Phys. Chem. Solids* **58** (1997) 319.
9. S.Y. Huang, L. Kavan, I. Exnar and M. Grätzel, *J. Electrochem. Soc.* **142** (1995) L142.
10. A. Hagfeldt, N. Vlachopoulos and M. Grätzel, *J. Electrochem. Soc.* **141** (1994) L82.
11. B. O'Regan and M. Grätzel, *Nature* **353** (1991) 737.
12. L.M. Peter, E.A. Ponomarev, G. Franco and N.J. Shaw, *Electrochim. Acta* **45** (1999) 549.
13. K. Tennakone, G.R.R.A. Kumara, I.R.M. Kottegoda, K.G.U. Wijayantha and V.P.S. Perera, *J. Phys. D: Appl. Phys.* **31** (1998) 1492.
14. A. Becquart, F. Cabané and P. Knauth, *J. Electroceramics* **1** (1997) 173.
15. P. Knauth, G. Albinet and J.-M. Debierre, *Ber. Bunsenges. Phys. Chem.* **102** (1998) 945.
16. J.-M. Debierre, P. Knauth and G. Albinet, *Appl. Phys. Lett.* **71** (1997) 1335.
17. D. Cahen, G. Hodes, M. Grätzel, J.-F. Guillemoles and I. Riess, *J. Phys. Chem. B* **104** (2000) 2053.
18. P. Knauth and Y. Massiani, *J. Electroanal. Chem.* **442** (1998) 229.
19. W. Büchner, R. Schliebs, G. Winter and K.-H. Büchel, 'Industrial Inorganic Chemistry', (VCH, Weinheim, 1989).
20. C. Noguera, 'Physique et Chimie des Surfaces d'Oxydes', (Aléa, Saclay, 1995).
21. J.-P. Jolivet, 'De la solution à l'oxyde, Savoirs Actuels', (Interéditions, Paris, 1994).
22. S.C. Liao, W.E. Mayo and K.D. Pae, *Acta Mater.* **45** (1997) 4027.
23. A.J. Bard and L.R. Faulkner, 'Electrochemical Methods – Fundamentals and Applications', (Wiley, New York, 1980).
24. J.R. Macdonald, 'Impedance Spectroscopy Emphasizing Solid Materials and Systems', (Wiley, New York, 1987).
25. W.M. Latimer, 'Oxidation Potentials', 2nd edn (Prentice Hall, New Jersey, 1952).
26. M.P. Cantao, J.I. Cisneros and R.M. Torresi, *J. Phys. Chem.* **98** (1994) 4865.
27. R. Van de Krol, Lithium Intercalation in Anatase, PhD thesis, Delft University of Technology, NL, 2000.
28. F.P. Koffyberg and F.A. Benko, *J. Appl. Phys.* **53** (1982) 1173.
29. R. van de Krol, A. Goossens and J. Schoonman, *J. Electrochem. Soc.* **144** (1997) 1723.
30. J.W. Orton, B.J. Goldsmith, J.A. Chapman and M.J. Powell, *J. Appl. Phys.* **53** (1982) 1602.
31. P. Knauth and H.L. Tuller, *Mat. Res. Soc. Symp. Proc.* **548** (1999) 429.